

**Copyright**

**by**

**Craig Ian White**

**2013**

The Thesis committee for Craig Ian White certifies that this is the  
approved version of the following thesis:

Higher precision mass measurement via the boundary of  
many-body phase space.

APPROVED BY  
SUPERVISING COMMITTEE:

Supervisor: \_\_\_\_\_

Can Kilic

\_\_\_\_\_

Duane Dicus

**Higher precision mass measurement via the boundary of  
many-body phase space.**

by

**Craig Ian White, B.S.**

Presented to the Faculty of the Graduate School

of the University of Texas at Austin

in Partial Fulfillment

of the Requirements

for the Degree of

**Master of Arts**

The University of Texas at Austin

December 2013

**Higher precision mass measurement via the boundary of  
many-body phase space.**

by

Craig Ian White, MA

The University of Texas at Austin, 2013

SUPERVISOR: Can Kilic

**Abstract**

We introduce a new method of mass measurement for particles in decay chains. The method relies upon performing a likelihood analysis on the phase space of the decay in its full dimensionality in a Lorentz-invariant formulation. This method is applicable for any decay chain, but we demonstrate it specifically in the case of a four-body final state decay in which one of the final particles is invisible. We directly compare our method to the edge and endpoint method and show that our new method can achieve higher precision with limited statistics.

# Contents

<b>1</b>	<b>Introduction</b> . . . . .	<b>1</b>
<b>2</b>	<b>Background</b> . . . . .	<b>3</b>
<b>3</b>	<b>Four-body phase space</b> . . . . .	<b>12</b>
<b>4</b>	<b>Mass measurements</b> . . . . .	<b>14</b>
<b>5</b>	<b>Results</b> . . . . .	<b>23</b>
<b>6</b>	<b>Conclusions</b> . . . . .	<b>28</b>
	<b>References</b> . . . . .	<b>29</b>

## List of Tables

1	2+2+2 Results Table . . . . .	24
2	2+3 Results Table . . . . .	26

## List of Figures

1	Dalitz plot . . . . .	4
2	Three-body decay . . . . .	5
3	2+2 decay chain . . . . .	5
4	Endpoint . . . . .	5
5	Edge . . . . .	6
6	2+2+2 decay chain . . . . .	10
7	2+2+2 Results . . . . .	25
8	2+3 Results . . . . .	27

# 1 Introduction

With the advent of the LHC, there now exists the potential to explore new physics beyond the standard model. We expect new physics for various theoretical reasons; one of which is the so-called hierarchy problem. Essentially the hierarchy problem asks why the scale of electroweak-symmetry breaking appears to be fine tuned. One of the most popular solutions to this problem is supersymmetry, which implies that there should be new particles close to the TeV scale. Such theories also typically imply the existence of weakly-interacting, massive particles (WIMPs), which are suitable candidates for the so-called dark matter.

As of yet, however, no trace of new physics has been found. This implies that, should new physics be found, it will only display itself in limited statistics. This magnifies the difficulties in the detection of new particles. Various theoretical issues also increase the difficulty of the detection of new particles. This is because most extensions of the Standard Model are dominated by  $\mathcal{Z}_2$  symmetry. Once  $\mathcal{Z}_2$ -odd particles are produced in pairs, they will decay through two and three-body decays until stable  $\mathcal{Z}_2$  particles are produced which escape detection. Given both these issues, it becomes important to optimize mass measurements given a relatively low number of events. While there are already numerous mass measurement methods, none of these work particularly well at low statistics, and several of them are computationally expensive. We will demonstrate a new method that works well at low statistics. Our method achieves this by determining the boundary of the kinematically accessible phase space in its full dimensionality. In addition our method is sensitive to shifts in the entire

spectrum, something that present methods are not sensitive to.

## 2 Background

Given the importance of mass measurements, it is not surprising that numerous measurement methods have been contrived. They rely upon an analysis of the phase space of the particles produced by the decay chain. In order to improve upon current methods, we first digress into the phase space of decay chains.

We will start by studying the dimensionality of the phase space. As an example, let us consider the simplest possible case: a single particle decaying into two. Since each particle has a four-momentum, there are in principle as many as eight degrees of freedom in the final state. The fact that the energy is fixed in terms of the momentum reduces the dimensionality of the phase space by 2. Now we are down to 6. We then have the constraint of energy-momentum conservation which reduces the degrees of freedom by four, so we are down to 2. Finally, we have rotational freedom to define our system of coordinates (this enables us to reduce our degrees of freedom by up to three), thus reducing our degrees of freedom to none. Thus the two-body decay is entirely constrained, or to put it another way all two-body decays have the same kinematics.

The three-body decay is somewhat different. Here a single particle decays into three particles, so we have as many as twelve degrees of freedom. Here again the energy is fixed in terms of the momentum, reducing the freedoms by 3. Again we also have energy-momentum conservation to fulfill, further reducing the degrees of freedom by 4. So now we have 5 degrees of freedom. Finally rotational freedom allows us to reduce the dimensionality by 3, yielding a final

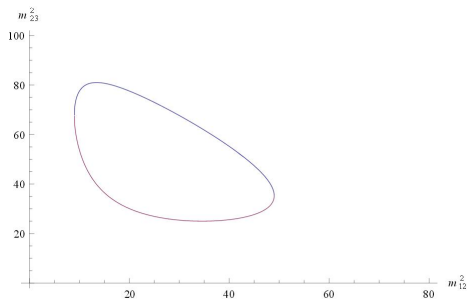


Figure 1: A Dalitz plot obtained from a three-body decay. Here we have used the parameters  $M = 10$  GeV,  $m_1 = 1$  GeV,  $m_2 = 2$  GeV,  $m_3 = 3$  GeV.

value of 2 degrees of freedom. Extending this analysis to an arbitrary number of particles it can be seen that the dimensionality of an  $n$ -particle phase space is  $3n - 7$ : the expected value of  $4n$  is reduced by  $n$  due to the constraint of the fixed energy in terms of the momentum, by 4 given momentum conservation, and by 3 due to rotational invariance. This yields a dimensionality of  $3n - 7$ , or 2 for the three-body case.

To describe the three-body decay we thus need two variables. We will choose a Lorentz-invariant parametrization. Our choice will be  $(p_i + p_j)^2 = m_{ij}^2$ , the sum of any two daughter-particle momenta. In 3-body decay, there are three such variables:  $m_{12}^2$ ,  $m_{13}^2$ , and  $m_{23}^2$ . Since we have only two degrees of freedom, we can eliminate one and choose any two as our independent variables, such as  $m_{12}^2$  and  $m_{23}^2$ . If we make a graph of these two variables, we produce what is called the Dalitz plot.

The Dalitz plot is key to the edge and endpoint method, one of the key mass

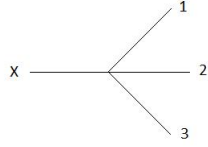


Figure 2: A graph of simple three-body decay without any intermediate resonances.

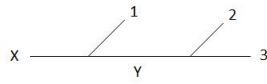


Figure 3: A graph of a three-body decay with an intermediate resonance. It is labeled as the 2+2 case.

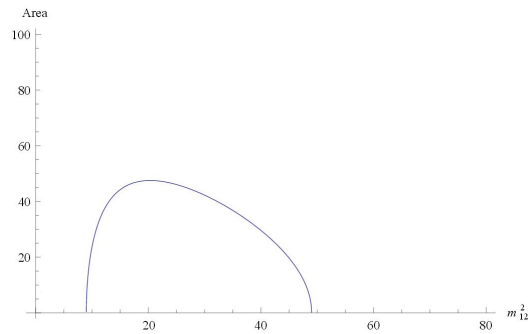


Figure 4: An example of an endpoint. Endpoints are found by projecting the phase space of the Dalitz plot onto the  $m_{12}^2$  axis. The parameters used are  $M = 10$  GeV,  $m_1 = 2$  GeV,  $m_2 = 2$  GeV,  $m_3 = 3$  GeV.

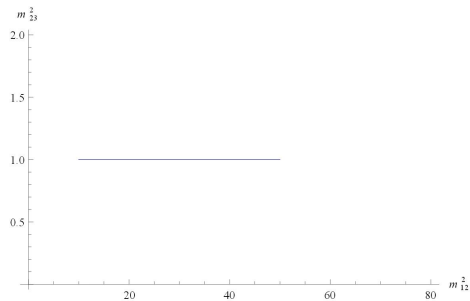


Figure 5: An edge. Edges are typically produced in 2+2 decays. Here  $m_{23}^2$  only takes one value since we have an additional constraint. The edge is then formed by projecting the phase space of the Dalitz plot onto the  $m_{12}^2$  axis. The parameters used here are  $M = 10$  GeV,  $m_1 = 1$  GeV,  $m_2 = 2$  GeV,  $m_3 = 3$  GeV.

measurement methods. To see what an edge or endpoint is, assume one of the final particles is invisible, say particle 3. Then we are not able to graph  $m_{23}$ , instead all we can do is measure the projection of the phase space of the Dalitz plot onto  $m_{12}$ . An example of this can be seen in Figure 4. This form is called an endpoint.

We shall now derive a formula for the position of endpoints. Given the definitions of  $m_{ij}^2$  (and defining  $M$  as the mass of the mother particle), we have

$$m_{12}^2 = (p_1 + p_2)^2 = (P - p_3)^2, \quad (1)$$

$$m_{23}^2 = (p_2 + p_3)^2 = (P - p_1)^2, \quad (2)$$

$$m_{13}^2 = (p_1 + p_3)^2 = (P - p_2)^2. \quad (3)$$

The endpoint is located at the maximum value of  $m_{12}$ . To find this we expand

the right-hand side of equation 1. This yields

$$m_{12}^2 = M^2 + m_3^2 - 2P \cdot p_3. \quad (4)$$

We are analyzing this in the rest frame of the mother particle. This gives us

$$m_{12}^2 = M^2 + m_3^2 - 2ME_3. \quad (5)$$

The maximal value of  $m_{12}$  occurs when  $m_3$  have no momentum. In this case equation 5 becomes

$$(m_{12}^2)_{max} = M^2 + m_3^2 - 2Mm_3 = (M - m_3)^2. \quad (6)$$

Thus, we obtain the final value for the endpoint:

$$(m_{12})_{max} = M - m_3. \quad (7)$$

So much for endpoints. There is, however, another way to get three daughter particles out of one mother particle. In this case, the mother particle decays into two particles, one of which further decays into two daughter particles, leaving a total of three daughter particles. This case is known as a 2+2 decay. An example of this is given in Figure 3. This case will be different, however, because as was previously argued all two-body decays are kinematically the same. Because of this only a small portion of the total Dalitz plot will be sampled. This results in a very different shape when the plot is collapsed down to one dimension. This is called an edge (see Figure 5).

Let us now derive a formula for the position of the edges. This has been well studied in the literature [1-14]. We will work in the rest frame of  $Y$ , in which  $\vec{q}$

is the 3-momentum of  $X$  and 1, while  $\vec{k}$  is the 3-momentum of 2 and 3. From energy conservation for the first decay

$$\sqrt{m_X^2 + \vec{q}^2} = \sqrt{m_1^2 + \vec{q}^2} + m_Y \quad (8)$$

$$|\vec{q}| = \frac{\sqrt{m_1^4 + (m_X^2 - m_Y^2)^2 - 2m_1^2(m_X^2 + m_Y^2)}}{2m_Y}. \quad (9)$$

Likewise, energy conservation for the second decay allows us to find  $\vec{k}$  and yields

$$\sqrt{m_2^2 + \vec{k}^2} + \sqrt{m_3^2 + \vec{k}^2} = m_Y \quad (10)$$

$$|\vec{k}| = \frac{\sqrt{m_2^4 + (m_Y^2 - m_3^2)^2 - 2m_2^2(m_Y^2 + m_3^2)}}{2m_Y}. \quad (11)$$

We can now parametrize our variables in terms of Lorentz-invariant quantities;

we will use the already introduced  $m_{ij}^2 = (p_i + p_j)^2$ . Now we can compute  $m_{12}$ .

Based upon the conservation of momentum:

$$\begin{aligned} m_{12}^2 &= m_1^2 + m_2^2 + m_3^2 + m_X^2 - m_Y^2 - m_{31}^2 \\ &= m_1^2 + m_2^2 + m_3^2 + m_X^2 - m_Y^2 - \\ &\quad \left( \left( \sqrt{\vec{k}^2 + m_3^2} + \sqrt{\vec{q}^2 + m_1^2} \right)^2 - (\vec{k} + \vec{q})^2 \right) \end{aligned} \quad (12)$$

As can be seen from the previous equation, if  $\vec{k}$  and  $\vec{q}$  are anti-parallel  $m_{12}^2$  is

maximized. Plugging this in yields the position of the edge:

$$\begin{aligned}
m_{12}^2 = & \frac{1}{2m_Y^2} (m_2^2 (m_X^2 + m_Y^2) \\
& + (m_X - m_Y)(m_X + m_Y)(m_Y - m_3)(m_Y + m_3) \\
& + [(m_1 - m_X - m_Y)(m_1 + m_X - m_Y)(m_1 - m_X + m_Y) \\
& (m_1 + m_X + m_Y)(-m_2 + m_Y - m_3)(m_2 + m_Y - m_3) \\
& (-m_2 + m_Y + m_3)(m_2 + m_Y + m_3) \\
& + m_1^2 (-m_2^2 + m_Y^2 + m_3^2)^{\frac{1}{2}}.
\end{aligned} \tag{13}$$

This equation is quite complex; it can be simplified by making the assumption that  $m_1 \simeq m_2 \simeq 0$ . We have verified numerically that this assumption is justified in our case. This greatly simplifies our equation to

$$(m_{12}^2)_{max} = \frac{(M^2 - m_Y^2)(m_Y^2 - m_3^2)}{m_Y^2}. \tag{14}$$

So much for three-body decay. In this paper we will be looking mostly at four-body decay. We will look at a full analysis of four-body phase space in the next section. For now, we consider two possible cases. In the first, an initial mother particle decays into two daughter particles, one of which decays into two further particles, one of which decays yet again into two particles. This process is referred to as the 2+2+2 case. The other case we will be examining is known as the 2+3 case. Here a mother particle decays into two daughter particles, one of which then decays into three particles. A diagram of these decays is shown in Figure 6.

We can write formulas for edges and endpoints in these four-body cases as well. Full derivations of this are given in [3] and [5]. Note that this requires us



Figure 6: A graph of the two cases of four-body decay that we will be considering. They are referred to as the 2+2+2 case and the 2+3 case, respectively.

to make the approximation  $m_1 = m_2 = m_3 \simeq 0$ . We have numerically verified that this approximation is valid for our case. Finally, this gives us the formulas for edges and endpoints. For the 2+2+2 case,

$$(m_{123}^2)_{max} = \begin{cases} \frac{(m_X^2 - m_Y^2)(m_Y^2 - m_4^2)}{m_Y^2} & \frac{m_X}{m_Y} > \frac{m_Y}{m_Z} \frac{m_Z}{m_4} \\ \frac{(m_X^2 m_Z^2 - m_Y^2 m_4^2)(m_Y^2 - m_Z^2)}{m_Y^2 m_Z^2} & \frac{m_Y}{m_Z} > \frac{m_Z}{m_4} \frac{m_X}{m_Y} \\ \frac{(m_X^2 - m_Z^2)(m_Z^2 - m_4^2)}{m_Z^2} & \frac{m_Z}{m_4} > \frac{m_X}{m_Y} \frac{m_Y}{m_Z} \\ (m_X - m_4)^2 & \text{otherwise} \end{cases} \quad (15)$$

The equations for  $m_{ij}^2$  are very similar to  $m_{23}^2$  in the three-body case.

$$(m_{23}^2)_{max} = (m_Y^2 - m_Z^2)(m_Z^2 - m_4^2) / m_Z^2, \quad (16)$$

$$(m_{12}^2)_{max} = (m_X^2 - m_Y^2)(m_Y^2 - m_Z^2) / m_Y^2, \quad (17)$$

$$(m_{13}^2)_{max} = (m_X^2 - m_Y^2)(m_Z^2 - m_4^2) / m_Z^2. \quad (18)$$

For the 2+3 topology, there is no distinction between particles 2 and 3, so the kinematics must exhibit a symmetry between 2 and 3,

$$(m_{123}^2)_{max} = \begin{cases} \frac{(m_X^2 - m_Y^2)(m_Y^2 - m_Z^2)}{m_Y^2} & \frac{m_X}{m_Y} > \frac{m_Y}{m_4} \\ (m_X - m_4)^2 & \text{otherwise} \end{cases} \quad (19)$$

$$(m_{23}^2)_{max} = (m_Y - m_4)^2, \quad (20)$$

$$(m_{12}^2)_{max} = (m_{13}^2)_{max} = (m_X^2 - m_Y^2)(m_Y^2 - m_4^2)/m_Y^2. \quad (21)$$

So far we have explained the edge and endpoint method of mass measurement. This is because it is the method we will use to directly compare to our new method, which will rely on a full-dimensional phase space analysis. There are other methods of mass measurement that rely upon methods that are not fully Lorentz invariant but are invariant under boosts along the beam direction (useful in the context of hadron colliders). An example of such a method is the  $M_{T2}$  method, which is examined in [15-21]. Another is the “polynomial” method. This method is most useful for those decay chains which are possible to solve analytically. This makes it very useful in the case of the 2+2+2 decay chain. However, our method is superior for the 2+3 decay chain. Further discussion of the polynomial method can be found in [14], [22], and [23].

### 3 Four-body phase space

In this thesis we will be dealing mainly with four-body problems, so we now consider four-body phase space. Based upon our previous analysis, the phase space will have a dimensionality of  $3n - 7$ , or 5 in the specific case of four-body decay. For now, we will rely on the Lorentz-invariant  $p_i \cdot p_j = z_{ij}$  as our variables of choice. To organize this formalism, we will introduce the matrix  $\mathcal{Z} = \{m_{ij}\}$ . Since we have only 5 degrees of freedom, not all of the  $z_{ij}$  are independent. Introducing  $\mathcal{Z}$  allows us to define

$$\Delta_l = (-1)^{l-1} \sum \text{determinant of all } l \times l \text{ diagonal minors of } \mathcal{Z}, \quad (22)$$

which will become important shortly.

A phase space density is expressed in terms of a differential volume element for each degree of freedom. So our volume element should have  $\prod_{i < j} dz_{ij}$  with six terms, which will be reduced to five do to the presence of a delta function expressing momentum conservation. In general the reduction of degrees of freedom from  $n(n-1)/2$  to five will be expressed by the inclusion of a number of Dirac- $\delta$  functions.

Beyond this simple overview, the full derivation of the Lorentz invariant volume element of four-body phase space is surprisingly nontrivial. The full derivation is given in [24]. Here, we will only cite the results. Switching to the set of variables  $m_{ij}^2 = (p_i + p_j)^2$ , the volume element of four-body phase space is

$$d\Pi_4 = \left( \prod_{i < j} dm_{ij}^2 \right) \frac{C}{M_X^2 \Delta_4^{1/2}} \delta \left( \sum_{i < j} m_{ij}^2 - K \right), \quad (23)$$

where

$$C = \frac{8}{(4\pi)^{10}}, \quad K = M_X^2 + 2 \sum_{i=1}^4 m_i^2. \quad (24)$$

Note that  $M_X$  is the mass of the mother particle. Note that unlike 3-body phase space this is not a constant: it depends upon  $\Delta_4$  which depends upon the kinematics of the event. [24] discusses the boundary of the kinematically accessible region. For  $n \geq 4$ , the kinematically accessible region is defined by the conditions

$$\Delta_l > 0 \text{ for } l \leq 4 \quad (25)$$

and

$$\Delta_l = 0 \text{ for } l > 4 \quad (26)$$

with the boundary of the physical region corresponding to  $\Delta_4 = 0$ .

## 4 Mass measurements

Now that we have covered the basic theory of particle decay, we will discuss our method of mass measurements in detail. In this case, we will be looking a four-body decay (either the 2+2+2 or the 2+3 decays). For a given data set of the masses of the final particles (we will label them as particles 1–4 with particle 4 being invisible), we will be looking for the mass values of the intermediate particles and the invisible particle (labeled  $X, Y, Z$  and 4). To do this in our phase-space method, we will determine a likelihood for each hypothesized mass value of the intermediate particles.

What is needed, then, is the probability that a given mass hypothesis fits the given data. Mathematically, this can be represented as follows: the probability of some event  $A$  to occur given that  $A$  is dependent upon another event  $B$  occurring is labeled as  $P(A, B)$ . This is equal to the probability of  $B$  times the probability of  $A$  given that  $B$  occurs, or expressed mathematically

$$P(A, B) = P(B) P(A|B). \quad (27)$$

If  $A$  and  $B$  are symmetric, then

$$P(B) P(A|B) = P(A) P(B|A). \quad (28)$$

Recasting this in our language leads to

$$P(data) P(\{m\}|data) = P(\{m\}) P(data|\{m\}). \quad (29)$$

This equation should be read as the probability of the data multiplied by the probability of a particular mass hypothesis given the data is equal to the prob-

ability of the mass hypothesis multiplied by the probability of the data given the mass hypothesis. This equation can be rearranged to yield

$$P(\{m\}|data) = \frac{P(\{m\})}{P(data)} P(data|\{m\}) \quad (30)$$

This solves for what we are interested in: namely the probability of the mass hypotheses given the data. Now, it is not known how to compute the probability of the data nor the probability of the mass hypotheses in isolation. However, this is not necessary as these two quantities can be treated as constants for our purposes. This leads us to the result

$$P(\{m\}|data) \propto P(data|\{m\}). \quad (31)$$

This we can indeed calculate.

The probability is proportional to the differential width, which is equal to the phase-space density times the amplitude of the decay:

$$d\Gamma = \frac{1}{2m_X} d\Pi_4 |\mathcal{M}|^2. \quad (32)$$

Again,  $d\Pi_4$  is the four-body phase space from equation 23. What the amplitude  $|\mathcal{M}|^2$  looks like will depend upon whether we are in the 2+2+2 decay case or the 2+3 decay case.

Let us start with the 2+2+2 case. Here the amplitude is proportional to the  $Y$  and  $Z$  propagators,

$$|\mathcal{M}|^2 \propto \frac{1}{|m_Y^2 - (p_2 + p_3 + p_4)^2 + im_Y \Gamma_Y|^2} \frac{1}{|m_Z^2 - (p_3 + p_4)^2 + im_Z \Gamma_Z|^2}, \quad (33)$$

where the  $\Gamma$ s are the widths of their respective particles. However, usage of the

narrow width approximation results in the following simplifications,

$$\frac{1}{|m_Y^2 - (p_2 + p_3 + p_4)^2 + im_Y \Gamma_Y|^2} \simeq \delta(m_{23}^2 + m_{24}^2 + m_{34}^2 - K_Y) \frac{\pi}{m_Y \Gamma_Y} \quad (34)$$

where  $K_Y = m_Y^2 + m_2^2 + m_3^2 + m_4^2$ , and

$$\frac{1}{|m_Z^2 - (p_3 + p_4)^2 + im_Z \Gamma_Z|^2} \simeq \delta(m_{34}^2 - m_Z^2) \frac{\pi}{m_Z \Gamma_Z}. \quad (35)$$

Combining this simplified amplitude with the phase-space density we already reviewed, we can compute the total probability.

The phase space included a factor of  $\prod dm_{ij}^2$ , which in this instance has six terms:  $m_{12}^2, m_{13}^2, m_{14}^2, m_{23}^2, m_{24}^2$ , and  $m_{34}^2$ . The phase space itself has one delta function that can eliminate one variable, and the amplitude in this case has two such delta functions. This allows us to reduce the total number of variables to three. This is convenient because it allows us to eliminate the terms involving particle four (which may be invisible in our scheme):  $m_{14}^2, m_{24}^2$ , and  $m_{34}^2$ .

All this allows us to write the probability of obtaining an event given a particular mass hypothesis  $\{m_\sigma\}$

$$\mathcal{L}(m_\sigma, m_{ij}^2) = \frac{1}{\Gamma_X} \frac{1}{2m_X} \mu_{XY1}^2 \mu_{YZ2}^2 \mu_{Z34}^2 \frac{\pi}{m_Y \Gamma_Y} \frac{\pi}{m_Z \Gamma_Z} \frac{1}{(4\pi)^6} \frac{1}{2m_X^2} \Theta(\Delta_4) \frac{1}{\Delta_4^{1/2}}. \quad (36)$$

A few explanations are in order. The initial factor  $\frac{1}{\Gamma_X}$  is a normalization that ensures that the probability is one when integrated over all possible values (remember particle  $X$  is the mother particle). The  $\frac{1}{2m_X}$  comes from the definition of a differential width. The factors of  $\mu$  are trilinear couplings (the subscripts represent which particles are coupled) that come from the amplitude. Finally,

the  $\Theta$  function ensures that any value that falls outside the physically allowed region is excluded.

We use the likelihood to determine the best mass hypothesis in a given number of events. Each of set of events is called a pseudo-experiment. We then do many pseudo-experiments to get a distribution of winning mass hypotheses. To obtain a probability for the whole sample, we must multiply the probabilities obtained from each individual event. Thus,

$$\mathcal{L}(m_\sigma) = \prod_{events} \mathcal{L}(m_\sigma, m_{ij}^2). \quad (37)$$

However, to avoid minute probabilities (the type that computers are likely to round off to zero), we will take the log of each probability and sum them, which is mathematically equivalent.

The 2+3 case is a little more complicated, for now we have lost one of our on-shell constraints. So we now have four degrees of freedom, but we still only have three known variables (particle four is still invisible). This means our likelihood function will include an integration over the additional variable. This yields a similar, but somewhat different, likelihood function

$$\mathcal{L}(m_\sigma, m_{ij}^2) = \frac{1}{\Gamma_X} \int dm_{34}^2 \frac{1}{2m_X} \mu_{XY}^2 \lambda_{Y234}^2 \frac{\pi}{m_Y \Gamma_Y} \frac{1}{m_Y \Gamma_Y} \frac{1}{(4\pi)^6} \frac{1}{2m_X^2} \Theta(\Delta_4) \frac{1}{\Delta_4^{1/2}}. \quad (38)$$

Note that this probability is quite similar to the first one, having many of the same terms. It differs only by having a quartic coupling  $\lambda$  in place of the trilinear coupling of the previous equation, and in the presence of the integral over  $m_{34}^2$ .

It is possible to perform this integral analytically. This can be done by

switching variables from  $m_{ij}^2$  to  $\{m_{12}, m_{23}, m_{123}, m_{34}\}$ . In this basis,  $\Delta_4$  may be written as

$$\Delta_4 = \frac{1}{16} (am_{34}^4 + bm_{34}^2 + c). \quad (39)$$

Given this, the range of the  $m_{34}^2$  integral is from  $s_{34}^-$  to  $s_{34}^+$ . Where,

$$s_{34}^\pm = -\frac{b}{2a} \pm \frac{\sqrt{b^2 - 4ac}}{2a}. \quad (40)$$

The functional forms of the constants  $a, b, c$  are expressed below:

$$a = \lambda(m_1^2, m_{23}^2, m_{123}^2), \quad (41)$$

$$b = 2\text{Det} \begin{bmatrix} 2m_{23}^2 & m_{123}^2 + m_{23}^2 - m_1^2 & m_{23}^2 - m_Y^2 + m_4^2 \\ m_{123}^2 + m_{23}^2 - m_1^2 & 2m_{123}^2 & m_{123}^2 - m_X^2 + m_4^2 \\ m_{23}^2 - m_2^2 + m_3^2 & m_{123}^2 - m_{12}^2 + m_3^2 & m_3^2 + m_4^2 \end{bmatrix} \quad (42)$$

$$b^2 - 4ac =$$

$$16G(m_{12}^2, m_{23}^2, m_{123}^2, m_2^2, m_1^2, m_3^2) G(m_{123}^2, m_Y^2, m_X^2, m_{23}^2, m_1^2, m_4^2). \quad (43)$$

Here we have introduced the functions  $\lambda$  and  $G$  which are defined as such

$$\lambda(X, Y, Z) = X^2 + Y^2 + Z^2 - 2XY - 2YZ - 2ZX, \quad (44)$$

$$\begin{aligned} G(X, Y, Z, U, V, W) = & XY(X + Y - Z - U - V - W) + \\ & ZU(Z + U - X - Y - V - W) + \\ & VW(V + W - X - Y - Z - U) + XZW + YZW + YUW. \end{aligned} \quad (45)$$

Solving the integral in this basis results in

$$\mathcal{L}(m_\sigma, m_{ij}^2) = \frac{1}{\Gamma_X} \frac{1}{2m_X} \mu_{XY}^2 \lambda_{Y234}^2 \frac{\pi}{m_Y \Gamma_Y} \frac{1}{(4\pi)^5} \frac{1}{2m_X^2} \frac{1}{\sqrt{\lambda_0}} \Theta(-G_1) \Theta(-G_2), \quad (46)$$

where

$$\lambda_0 = (m_1^2, m_{23}^2, m_{123}^2), \quad (47)$$

$$G_1 = G(m_{12}^2, m_{23}^2, m_{123}^2, m_2^2, m_1^2, m_3^2), \quad (48)$$

$$G_2 = G(m_{123}^2, m_Y^2, m_X^2, m_{23}^2, m_1^2, m_4^2). \quad (49)$$

The method for determining likelihoods is unchanged from the 2+2+2 case, so in the 2+3 case we will also use a large number of events to form into a number of samples. We will then find the total likelihood:

$$\mathcal{L}(m_\sigma) = \prod_{events} \mathcal{L}(m_\sigma, m_{ij}^2). \quad (50)$$

We will now compare the results obtained through the traditional method of using edges and endpoints with our new method utilizing four-body phase space. For the 2+2+2 topology,  $Y$  and  $Z$  are on-shell, this means that  $m_{12}^2$  and  $m_{23}^2$  have edges. By contrast,  $m_{13}^2$  and  $m_{123}^2$  have endpoints. We can define the quality-of-fit variable for any mass hypothesis for each set of events as

$$Q = \left( \sum_{i=endpts.} \left( \frac{O_{i,predicted} - O_{i,measured}}{O_{i,measured}} \right)^2 \right) \mathcal{F}. \quad (51)$$

Here  $O$  represents the predicted and measured positions of each edge and endpoint.  $\mathcal{F}$  is a function that is defined to be equal to one if the positions of the (measured) edges and endpoints are smaller than the predicted ones. Otherwise

$\mathcal{F}$  is equal to zero. Thus, it performs much the same role as the step function in the phase-space analysis.

For the 2+3 case, we no longer have an on-shell condition due to  $Z$ . This turns  $m_{12}^2$  and  $m_{23}^2$  from edges to endpoints. Otherwise, the definition of quality of fit is not different.

For our likelihood method, let's start with the 2+2+2 decay chain. We will work with the spectrum

$$\begin{aligned} M_X &= 500\text{GeV}, & M_Y &= 350\text{GeV}, \\ M_Z &= 200\text{GeV}, & M_4 &= 100\text{GeV}, \\ m_1 &= m_2 = m_3 = 5\text{GeV}, \end{aligned} \tag{52}$$

and for each "experiment" we will use 100 events. We will scan our hypotheses over a tilted lattice of the form

$$m_\sigma = M_+ (100\text{GeV}) \left( \alpha V_{(1)\sigma} + \beta V_\sigma^{(2)} + \gamma V_\sigma^{(3)} + \delta V_\sigma^{(4)} \right), \sigma = X, Y, Z, 4, \tag{53}$$

where

$$\begin{aligned} V_\sigma^{(1)} &= \{1, 1, 1, 1\}, \\ V_\sigma^{(2)} &= \{1, -1, 0, 0\}, \\ V_\sigma^{(3)} &= \{1, 1, -1, -1\}, \\ V_\sigma^{(4)} &= \{0, 0, 1, -1\}. \end{aligned} \tag{54}$$

Here  $V(1)$  corresponds to the flat direction. For the phase space analysis, we will scan over a very small range of values:

$$\alpha \in [-1.5 \times 10^{-2}, 1.5 \times 10^{-2}] \tag{55}$$

and

$$\beta, \gamma, \delta \in [-1.5 \times 10^{-3}, 1.5 \times 10^{-3}]. \tag{56}$$

We now have a benchmark spectrum and a set of mass hypotheses. We may now proceed with the analysis described in the previous sections, both the edge and endpoint analysis and the phase space analysis, where we will use  $\mathcal{O}(10^3)$  pseudo-experiments. For the phase space analysis, as previously described, the winning value will be the mass hypothesis with the largest phase space density, determined by the likelihood.

For the 2+3 topology, we will use a similar method. Here our mass spectrum will be

$$\begin{aligned}
 m_X &= 500 \text{ GeV}, & m_Y &= 350 \text{ GeV}, & m_4 &= 100 \text{ GeV}, \\
 m_1 &= m_2 = m_3 = 5 \text{ GeV}.
 \end{aligned}
 \tag{57}$$

Again we will choose an off-axis set of mass hypotheses:

$$m_\sigma = M_\sigma + (100 \text{ GeV}) \left( \alpha V_\sigma^{(1)} + \beta V_\sigma^{(2)} + \gamma V_\sigma^{(3)} \right), \sigma = \{X, Y, 4\},
 \tag{58}$$

where

$$\begin{aligned}
 V_\sigma^{(1)} &= \{1, 1, 1\} \\
 V_\sigma^{(2)} &= \{0, 1, -2\} \\
 V_\sigma^{(3)} &= \{2, -1, -1\}.
 \end{aligned}
 \tag{59}$$

Here again,  $V_\sigma^{(1)}$  is the flat direction. Here our range to scan over is

$$\begin{aligned}
 \alpha &\in [-1, 1] \\
 \beta &\in [-0.1, 0.1] \\
 \gamma &\in [-0.05, 0.05].
 \end{aligned}
 \tag{60}$$

This is for the case where the number of events per pseudo-experiment is one hundred. We will also do this for the case where there are one thousand events

per pseudo-experiment. For this we will scan over a more appropriate range:

$$\begin{aligned}\alpha &\in [-3.5 \times 10^{-2}, 1.0 \times 10^{-2}] \\ \beta &\in [-4.0 \times 10^{-3}, 4.0 \times 10^{-3}] \\ \gamma &\in [-1.5 \times 10^{-3}, 0.5 \times 10^{-3}].\end{aligned}\tag{61}$$

For the endpoint method, the following numbers were chosen

$$\begin{aligned}\alpha &\in [-2.0, 2.0] \\ \beta &\in [-4.0 \times 10^{-2}, 4.0 \times 10^{-2}] \\ \gamma &\in [-2.0 \times 10^{-2}, 2.0 \times 10^{-2}].\end{aligned}\tag{62}$$

Again, our method for determining the likelihood is the same as the 2+2+2 decay chain: namely that the most likely mass hypothesis is determined by the value of our previously defined likelihood function.

## 5 Results

We proceeded to run both the phase space and endpoint analyses for one thousand pseudo-experiments. Here we will list the mean and standard deviation of the distribution of the winning mass hypotheses across pseudo-experiments (remember that each pseudo-experiment consists of one hundred events). We have also graphed the distributions for both the 2+2+2 and 2+3 decay chains. The difference between the two methods can be clearly seen from these graphs: the phase space method is decisively superior.

First we will analyze the 2+2+2 case as seen in Table 1. Note here the inaccuracy of the endpoint method compared to the phase space method. However, the endpoint method is not merely less accurate, but it also is much less sensitive than the phase space method as shown by its large error. By contrast, the values obtained by the phase space method is very tightly constrained. This can also be seen in Figure 7.

Now we will show the same results for the 2+3 decay chain. As can be seen from Table 2 and Figure 8, the difference between the two methods is dramatic and decisively in favor of the phase space method. Here, however, we perform the analysis twice. First, we will use pseudo-experiments of one hundred events each. Then we will do a second analysis using one thousand events per experiment. We do this to check our conclusions for low versus high statistics. Comparing the results shows that the endpoint method actually does quite well in the  $N = 1000$  case, however it does poorly in the  $N = 100$  case. This shows us that it requires higher statistics to work well. By contrast our

Mass (GeV)	Phase space	End-points
$m_X$	$499.89 \pm 0.60$	$677.41 \pm 157.47$
$m_Y$	$349.90 \pm 0.59$	$527.19 \pm 155.96$
$m_Z$	$199.92 \pm 0.59$	$380.11 \pm 160.57$
$m_4$	$99.93 \pm 0.65$	$277.87 \pm 156.42$
$\alpha$	$(-0.87 \pm 6.03) \times 10^{-3}$	$1.78 \pm 1.58$
$\beta$	$(-0.07 \pm 0.38)^{-3}$	$(0.11 \pm 1.54) \times 10^{-2}$
$\gamma$	$(-0.17 \pm 0.44) \times 10^{-3}$	$(-0.84 \pm 1.44) \times 10^{-2}$
$\delta$	$(-0.09 \pm 0.66) \times 10^{-3}$	$(1.12 \pm 3.08) \times 10^{-2}$

Table 1: The results for the 2+2+2 decay case. Note that the values for the phase space method are much closer to the actual values than the values obtained by endpoint method. The “error” here is the value of one standard deviation.

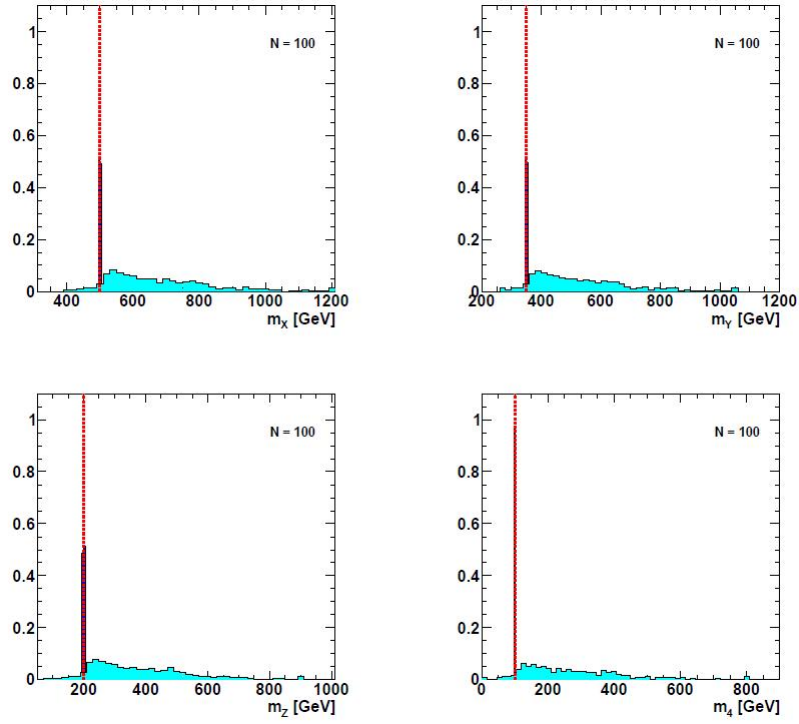


Figure 7: A graph of the distribution of the winning mass hypotheses for the phase space and endpoint analysis for the 2+2+2 decay chain. The dashed red line is the true value of the mass. The dark blue distribution is the phase space analysis and the light blue distribution represented the endpoint analysis.

Mass (Gev)	$N_{events} = 100$		$N_{events} = 1000$	
	Phase space	Endpoints	Phase space	Endpoints
$m_X$	$495.84 \pm 11.95$	$434.32 \pm 25.93$	$499.40 \pm 0.96$	$463.32 \pm 11.66$
$m_Y$	$345.69 \pm 12.13$	$284.11 \pm 28.48$	$349.39 \pm 0.97$	$312.94 \pm 12.08$
$m_4$	$96.86 \pm 13.97$	$37.61 \pm 27.45$	$99.56 \pm 1.08$	$63.83 \pm 11.91$
$\alpha$	$-0.039 \pm 0.127$	$-0.647 \pm 0.272$	$(-5.49 \pm 9.97) \times 10^{-3}$	$-0.37 \pm 0.12$
$\beta$	$-0.006 \pm 0.013$	$-0.017 \pm 0.020$	$(0.89 \pm 1.05) \times 10^{-3}$	$(-4.4 \pm 3.9) \times 10^{-3}$
$\gamma$	$-0.001 \pm 0.005$	$-0.005 \pm 0.012$	$(0.23 \pm 0.38) \times 10^{-3}$	$(-0.2 \pm 3.0) \times 10^{-3}$

Table 2: The mean and standard deviation of the 2+3 case, for both the  $N = 100$  and  $N = 1000$  cases.

method works well in both cases. Our results suggest that, in order for the endpoint method to converge on the right answer, it would need more statistics, perhaps on the order of  $N = 10000$ . However, the phase space method has already converged upon the answer in the  $N = 100$  case.

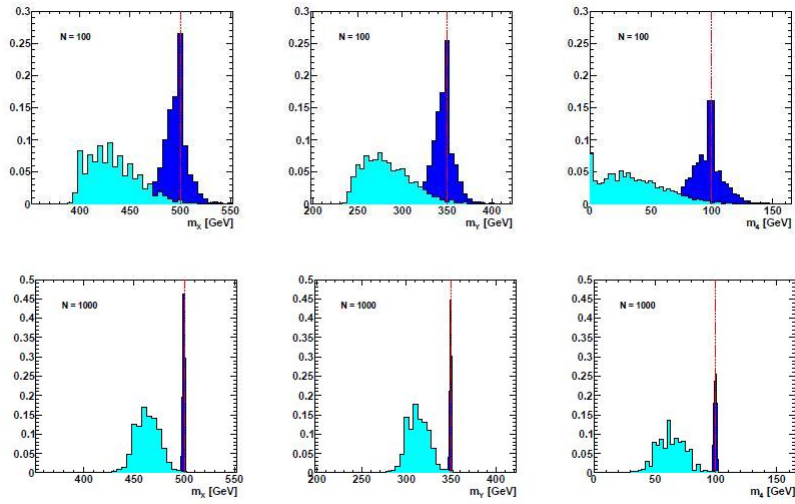


Figure 8: The distributions for the 2+3 decay cases. The top graphs are for the  $N = 100$  case, and the lower graphs are for the  $N = 1000$  case. Again, notice the much better fit of the phase-space method (dark blue) versus the endpoint method (light blue).

## 6 Conclusions

We have demonstrated that the phase space method provides significantly superior results to the endpoint method. This is especially true in the case of low statistics. This is important because we might be forced to use low statistics to test any future new physics. This is to be expected because some information is lost when the phase space is projected onto a one-dimensional observable, which happens when using edges or endpoints.

While our method is very useful, there are some areas for further study to improve its effectiveness, especially to simulate realistic conditions in particle accelerators. For instance, in this paper, we have assumed perfect energy resolution. Clearly, this is an approximation. Imperfect detectors can be taken into account by convoluting the likelihood with the response of the detector. The likelihood then has a tail beyond the boundary of phase space. We have also ignored the possibility of backgrounds in our analysis. However, it is entirely possible to modify the likelihood so that it is based upon a joint signal plus background hypothesis to be applicable to the more general case.

## References

- [1] M. Shapiro J. Soderqvist I. Hinchliffe, F. Paige and W. Yao. *Phys.Rev.*, D55(5520):hep-ph/9610544, 1997.
- [2] I. Hinchliffe H. Bachacou and F. E. Paige. *Phys.Rev.*, D62(015009):hep-ph/9907518, 2000.
- [3] M. A. Parker B. Allanach, C. Lester and B. Webber. *JHEP*, 0009(004):hep-ph/0007009, 2000.
- [4] C. G. Lester. Ph.d. thesis. University of Cambridge, 2001.
- [5] D. J. Miller B. Gjelsten and P. Osland. *JHEP*, 0412(003):hep-ph/0410303, 2004.
- [6] D. J. Miller B. Gjelsten and P. Osland. *JHEP*, 0506(015):hep-ph/0501033, 2005.
- [7] M. A. Parker C. G. Lester and M. J. White. *JHEP*, 0601(080):hep-ph/0508143, 2006.
- [8] P. Osland D. J. Miller and A. Raklev. *JHEP*, 0603(034):hep-ph/0510356, 2006.
- [9] C. G. Lester. *Phys.Lett.*, B655(39):hep-ph/0603171, 2007.
- [10] G. G. Ross and M. Serna. *Phys.Lett.*, B665(212):0712.0943, 2008.
- [11] D. R. Tovey. *JHEP*, 0804(034):0802.2879, 2008.

- [12] G. G. Ross A. J. Barr and M. Serna. *Phys.Rev.*, D78(056006):0806.3224, 2008.
- [13] A. Pinder A. J. Darr and M. Serna. *Phys.Rev.*, D79(074005):0811.2138, 2009.
- [14] B. Webber. *JHEP*, 0909(124):0907.5307, 2009.
- [15] Y. G. Kim W. S. Cho, K. Choi and C. B. Park. *Phys. Rev. Lett.*, 100(171801):0709.0288, 2008.
- [16] Y. G. Kim W. S. Cho, K. Choi and C. B. Park. *JHEP*, 0802(035):0711.4526, 2008.
- [17] B. Gripaios A. J. Barr and C. G. Lester. *JHEP*, 0802(014):0711.4008, 2008.
- [18] B. Gripaios A. J. Barr and C. G. Lester. *JHEP*, 0911(096):0908.3779, 2009.
- [19] K. T. Matchev M. Burns, K. Kong and M. Park. *JHEP*, 0903(143):0810.5576, 2009.
- [20] K. T. Matchev M. Burns and M. Park. *JHEP*, 0905(094):0903.4371, 2009.
- [21] Y. Kim W. Cho, K. Choi and C. Park. *AIP Conf. Proc.*, 1078(274), 2009.
- [22] I. W. Kim T. Han and J. Song. *Phys. Rev.*, D87(035003):1206.5633, 2013.
- [23] I. W. Kim T. Han and J. Song. *Phys. Rev.*, D87(035003):1206.5641, 2013.
- [24] N. Byers and C. N. Yang. *Rev. Mod. Phys.*, 36(595), 1964.